Engineering Structures 205 (2020) 109858

Contents lists available at ScienceDirect

Engineering Structures

journal homepage: www.elsevier.com/locate/engstruct

Structural performance of beam system with T-stub type slit damper

Hae-Yong Park[a], Sang-Hoon Oh[b,*]

[a] Seismic Research and Test Center at Pusan National University, Busandaehak-ro 49, Mulgeum, Yangsan, Kyungnam, Republic of Korea
[b] School of Architecture Engineering, Pusan National University, Busandaehak-ro 63-2, Geumjeong-gu, Busan, Republic of Korea

ARTICLE INFO

Keywords:
Damage controlled system
Steel slit damper
Connection detail
Yield strength ratio
Hysteretic model

ABSTRACT

In this study, the structural performance of a beam system with a beam-to-column connection-type damage-controlled system was investigated. First, a connection detail with improved geometry was proposed based on results obtained from previous studies. The proposed connection detail uses a horizontally arranged steel slit damper as an energy absorption device and consists of support elements to help the effective bending and shear behavior of the slit damper. The overall behavior characteristics are similar to the Simpson strong-tie connection; however, the energy absorption device of the proposed detail is installed only at the bottom of the beam, and the connector attached to the top of the beam functions as a rotational hinge. The strength formula of the beam system with a new connection detail was derived according to the mechanical behavior pattern. The stiffness formula of the beam system was proposed considering the geometric characteristics of the connection elements. For practical verification, a cyclic loading test was conducted on the beam-to-column connection with a T-stub type slit damper designed with appropriate strength. Nonlinear finite element analysis (FEA) was also conducted using the aspect ratio of the beam and damper strength as variables. The test and FEA results confirmed that the strength and stiffness of the beam system with the proposed connection detail exhibited responses similar to the predicted values. When the damper strength was designed to be lower than that of the beam, the deformation caused by the rotational behavior of the connection was concentrated on the damper according to the moment gradient generated in the flexural members. As the damper/beam yield strength ratio or rotation angle increased, the plasticity of the beam was found to gradually strengthen. A performance curve was derived from the relationship between the strength of the beam system and the damage to the beam according to the damper strength design conditions. It is expected that a moment-resisting frame that satisfies the requirements can be designed by applying this derived performance curve to low- and mid-rise steel buildings. Finally, the hysteretic model of the beam system with the proposed connection detail was developed through an approximation to a tri-linear model according to the design condition.

1. Introduction

As a method to reduce seismic damage, a damage-controlled system that uses steel hysteretic dampers has been widely used in countries such as the United States and Japan since the mid-1990s. This system has a stable hysteretic behavior and has been assessed as an economical earthquake-resistant method. In general, such steel hysteretic dampers are installed with various support elements in the planes formed by the beams and columns of a structure. Brace and stud types of support elements are commonly used in these structures. Dampers combined in parallel in a building can reduce the seismic responses by providing the building with additional horizontal stiffness and strength. In particular, they can reduce the damage to the parent members because they intensively dissipate the plastic energy caused by an earthquake [1,2]. Installing the existing in-plane damage-controlled system in typical commercial low- and mid-rise buildings, however, involves the following restrictions: The uniform locations of openings and variability of the wall space in commercial buildings make it difficult to install sufficient energy absorption devices. Moreover, owing to the relatively low weld quality, it is difficult to guarantee the structural performance of the weld zones between the support elements and the structural members [3]. This means that the seismic performance of the entire structure cannot be guaranteed even though it has devices that exhibit excellent energy absorption.

Thus, the damage-controlled system that directly connects the beams to the columns by bolted connections has been developed in countries such as Japan and the United States since the beginning of 2000. This helps to prevent brittle fracture at the weld zones of beam-

* Corresponding author.
E-mail address: osh@pusan.ac.kr (S.-H. Oh).

https://doi.org/10.1016/j.engstruct.2019.109858
Received 5 July 2019; Received in revised form 7 October 2019; Accepted 25 October 2019

to-column connections and facilitates the introduction of vibration control systems to typical low- and mid-rise structures. These details consist of upper and lower connectors to connect the beams to columns, similar to a T-stub connection. The energy absorption devices are included in the T-stem or T-flange element. If these connection details operate as expected for the rotational behavior of the connection, the plastic hinge in the connection occurs in the energy absorption device located at the end of the beam. Therefore, they can prevent the brittle fracture of the beam and can be utilized as the moment-resistance mechanism with the benefit of fastened bolts.

Accordingly, studies conducted by Takeuchi et al. [3,4] are representative studies in which an energy absorption device detail was placed on the T-stem. In the connection detail presented by them, the upper T-stub has a vertical rib and the lower T-stem has a cross-section cut to a specific length. The deformation by the rotational behavior is transferred to the column as the tensile compressive resistance at the cut cross-section of the lower T-stem creates a couple moment using the upper T-stub element as the rotation axis. This behavior pattern was the basis of the design concept of the follow-up studies. Simpson strong-tie-strong frame moment connection (SST), a complemented detail that used the same plate type damper, is the only partially restrained connection detail that was introduced to AISC 358 as intermediate moment frame (IMF) and special moment frame (SMF) connection detail [5]. The SST connection detail has cut cross-sections in the upper and lower T-stem parts and shear tab with slot holes. When rotational behavior occurs in the connection owing to seismic force, the couple moment is transferred to the column member through the tensile and compressive behavior of the cut T-stem. In this instance, the cross-section cut with appropriate design resists most of the deformation caused by the rotational behavior and plays the role of a structural fuse. Oh et al. [6] proposed a damage-controlled system that used the slit damper vertically connected to the beam bottom flange and conducted cyclic loading tests according to the strength parameters of the damper and the presence of a composite slab. Based on the test results, they reported that the use of the proposed connection detail shared the intensive damage to the slit damper and provided excellent deformation capacity to the connection even when the composite slab was considered. As another study case that applied the slit damper, Safari et al. [7] conducted numerical analysis on the beam-to-column connection models with slit dampers in the upper and lower flanges at the end of the beam, and they compared the performance efficiency according to the geometric arrangement of the slit dampers as well as the strength and ductility capacity of the connection according to the yield mechanism. Through the analysis results, they proposed a new improved connection detail with high energy absorption capacity. Oh et al. [8,9] proposed a complemented detail that can provide the structural safety of the connection against vertical external force after a fracture occurred to the plate type energy absorption device in the T-stem, and they analyzed the damage distribution according to the strength and stiffness relationship between the beam and the energy absorption device experimentally and analytically. Koetaka et al. [10] attached a U-shaped steel damper to the bottom flange of the beam and conducted a cyclic loading test on the beam-to-column connection. In this instance, the column was set as the weak-axis resistant to the loading direction. The test results confirmed that the hysteretic energy was intensively dissipated by the damper and the beam and column incurred no damage. MacRae et al. [11] proposed a sliding hinge joint system which has double friction surfaces at the beam bottom, and it showed that the joint dissipates energy on the friction surface and the resulting hysteresis loop demonstrates a low possibility of large permanent displacements through experimental verification.

Moreover, as a connection detail that placed an energy absorption device on the T-flange, Latour and Rizzano [12] conducted theoretical and experimental studies on a connection with X-shaped split tee flange. Consequently, it was verified that the connection was a semi-rigid connection detail capable of effectively playing the role of a moment-resistance frame without causing any brittle fractures to the beam end owing to the moment-shear interaction effect of the X-shaped split tee. Similarly, Bayat and Shekastehband [13] constructed a part of the T-flange as a strut element acting in the out-of-plane direction and compared it with a typical T-stub connection through analytical research.

All of the studies described above aimed to prevent the brittle fracture in the connection by placing energy absorption devices with special geometry at the beam end and allowing them to resist most of the deformation of the connection. The presented connected details were reported to act as moment-resistance mechanisms but most of them were also treated as partially restrained connection details. In addition, there are few cases that specifically presented the design range of the damper according to the structural relationship with the adjacent beam members. Therefore, it is still difficult to apply the beam-to-column connection-type damage-controlled system to typical buildings with various design requirements.

This study was conducted with focus on two issues. First, a new improved detail that can be easily understood in terms of the structure and secure reliability was proposed by referring to the results of previous studies. To accomplish this, a horizontally arranged steel slit damper was applied to the proposed connection detail. The steel slit damper was chosen as the energy absorption device because several previous studies [14–16] revealed that it had excellent ductility capacity and a reliable structural characteristics prediction formula. Second, the design range of the damper was assessed according to the strength, stiffness, and damage to the parent members required for the connections of ordinary low- and mid-rise steel buildings. The strength and stiffness prediction formulas of the beam system with the proposed connection detail were compared with the actual responses according to the mechanical behavior, and the damage distribution of the components was analyzed according to the damper/beam yield strength ratio. Moreover, the hysteretic model of the proposed connection system was obtained according to the set design concept. A cyclic loading test was conducted on the beam-to-column connections with the proposed detail and the results of nonlinear multivariate analysis were obtained in this study.

2. Proposal of complemented connection detail

2.1. Design concept

Fig. 1 shows the connection detail proposed in this study. The proposed connection detail has a design concept similar to that of the existing related connection details. In other words, the rotation of the connection is resisted by the couple moment due to the horizontal axial force of the T-stubs attached to the top and bottom of the beam. To complement the shortcomings of the existing related connection detail, the proposed detail has the following characteristics: (a) the geometry of the energy absorption device is set to the steel slit damper, which is arranged in a horizontal direction. The compressive behavior of the plate type damper involves overstrength due to the influence of the plate to prevent out-of-plane buckling; however, the slit damper provides the same resistance and superior ductility capacity in both directions. Moreover, when the slit damper is vertically arranged as the detail proposed by Oh et al. [6], the inherent horizontal ductility capacity of the slit damper can be lowered because the rotation of the beam involves not only the horizontal displacement in the flexure and shear directions of the damper but also the vertical displacement that causes tension and compression. In the proposed detail, an element that transfers the axial force is installed at the bottom of the lower T-stem to effectively transfer the axial force acting on the beam flange to the damper. The support elements on the periphery of the slit damper are resistant in the axial direction to the flexure and shear behavior of the damper. (b) The energy absorption device is installed in the lower connector and the upper T-stub plays the role of a rotational hinge for

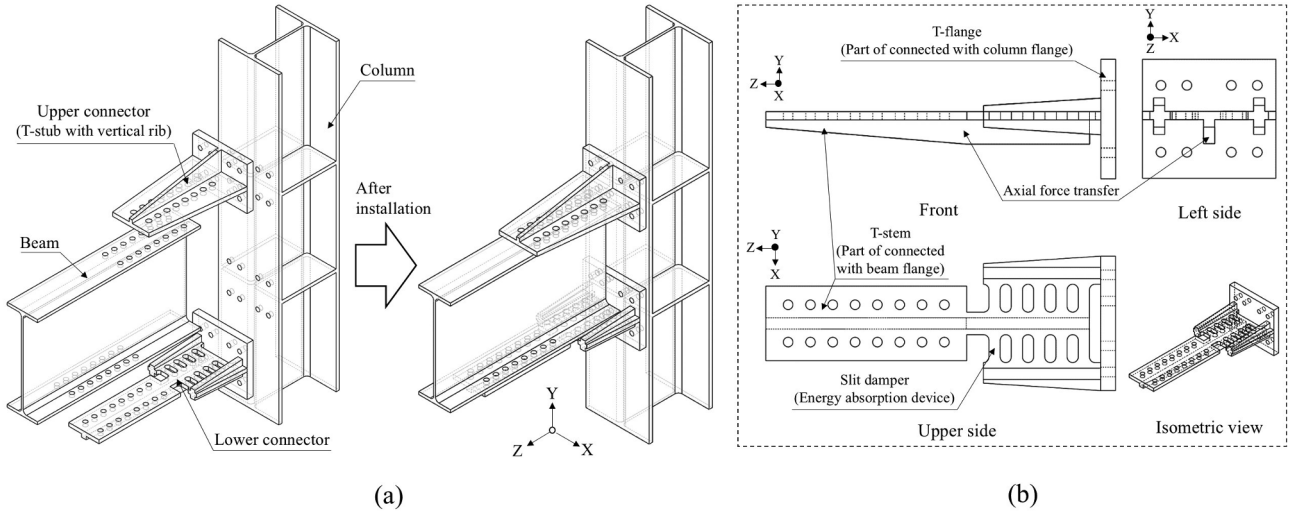

Fig. 1. Proposed connection detail: (a) whole shape and (b) lower connector detail.

the rotational behavior. This is different from the SST connection detail. Most of the related details address the upper and lower stress unbalance due to composite slab effects by attaching energy absorption devices only to the lower section (because the rotation axis exists in the upper T-stub), which makes it easy to observe the damage to the damper in the earthquake event. (c) A vertical rib is installed in the upper T-stub without installing shear tabs so that the shear force can be resisted by the moment-tension interaction between the upper T-stubs with vertical rib on both sides of the beam. For this purpose, the area of the vertical ribs attached to the T-flange shall be set larger than the area of the beam web. Hereafter, the proposed connection detail is referred to as the T-stub type slit damper (TSD) system due to its geometric characteristics.

2.2. Strength

2.2.1. Steel slit damper

The structural characteristics of the steel slit damper used in the proposed connection detail can be calculated referring the previous study [14]. For predicting the structural characteristics of the damper, the struts of the damper were idealized as shown in Fig. 3. The yielding load due to the flexure and shear behavior (Q_{yd}), the apparent maximum load (Q_{rd}) of the steel slit damper are expressed as follows from the geometric characteristics of a rectangular steel plate and using the above simplification.

$$Q_{yd} = min\left\{\frac{n\sigma_{yd}tB^2}{2H'}, \frac{2n\sigma_{yd}tB}{3\sqrt{3}}\right\};\ Q_{rd} = min\left\{\frac{n\sigma_{ud}tB^2}{2H'}, \frac{2n\sigma_{ud}tB}{3\sqrt{3}}\right\} \quad (1)$$

where n is the number of struts, t is the thickness of the damper, σ_{yd} and σ_{ud} are yielding and maximum tensile stress of the damper material. B, H′ represent the width of the strut and the equivalent height indicated in Fig. 3. In Eq. (1), the two terms in brackets indicate flexural yielding and shear yielding, respectively. The factor 2/3 in the second term of each bracket of Eq. (1) accounts for the fact that, within the elastic range, when the aspect ratio of the plate B/H is less than 1.0, the relationship between the average shear stress and the maximum shear stress is 2/3. The yield displacement of the steel slit damper, δ_{yd}, contains the displacement due to the flexural and shear deformation at the yielding load and can be simplified by the following elastic based equation [14].

$$\delta_{yd} = \frac{1.5Q_{yd}H_T}{nEtB}\left[\left(\frac{H'}{B}\right)^2 + 2.6\right] \quad (2)$$

Here E is the elastic modulus of the material and H_T means the total height of the strut defined in Fig. 3.

2.2.2. TSD beam system

The TSD beam system aims for the preceding plastic behavior of the damper for effective structural behavior. The moment of the beam system against the horizontal force is largest at the beam end. The preceding plasticity of the damper can be theoretically expected even when the yield strengths of the damper and beam are designed to be the same. However, because the ratio of the maximum strength of the slit damper to its yield strength is higher than the ratio of the full plastic moment of typical H-beam flexural members to its yield moment, the increase in the damper strength may involve the plastic behavior of the beam. Depending on the behavior pattern of the connection system, the yield moment of the TSD beam system M_{ybs} and the anticipated maximum moment M_{rbs} are affected by the yield ratio of the damper material, σ_{yd}/σ_{ud} and the span ratio (the effective length, L_{be}/the beam length, L_b). In this instance, they can be expressed as follows:

$$M_{ybs} = min\{Q_{yd}d, (M_{yb}/L_{be})L_b\};\ M_{rbs} = min\{Q_{rd}d, (M_{pb}/L_{be})L_b\} \quad (3)$$

where M_{yb} and M_{pb} denote the nominal yield moment and full plastic moment of the beam, and d denotes the distance between the centers of the upper and lower T-stems. The effective length, L_{be}, is defined as the distance from the center of the beam to the horizontal center point of the upper and lower bolt-fastening ends of the beam, as shown in Fig. 2.

2.3. Elastic stiffness

The bending stiffness of the TSD beam system, K_T, can be calculated as the series sum of the effective bending stiffness at the connector attachment section, K_C, and the bending stiffness of the beam for L_{be}, K_B, as shown in Fig. 4. K_C can be expressed as the series sum of the elastic axial stiffness by bending the upper and lower T-flanges, the axial elastic stiffness of non-yielding regions in the upper and lower T-stems, and the elastic stiffness of the slit damper. Therefore, the elastic stiffness formula of the TSD beam system can be expressed as follows:

$$K_T = \left(\frac{1}{K_C} + \frac{1}{K_B}\right)^{-1} \quad (4)$$

$$K_C = \left(\frac{1}{k_{uf}} + \frac{1}{k_{lf}} + \frac{1}{k_{us}} + \frac{1}{k_{ls1}} + \frac{1}{k_{ls2}} + \frac{1}{k_d}\right)^{-1} \quad (5)$$

$$K_B = \left(\frac{L_{be}^3}{3EI_b} + \frac{L_{be}}{A_{bw}G}\right)^{-1} \quad (6)$$

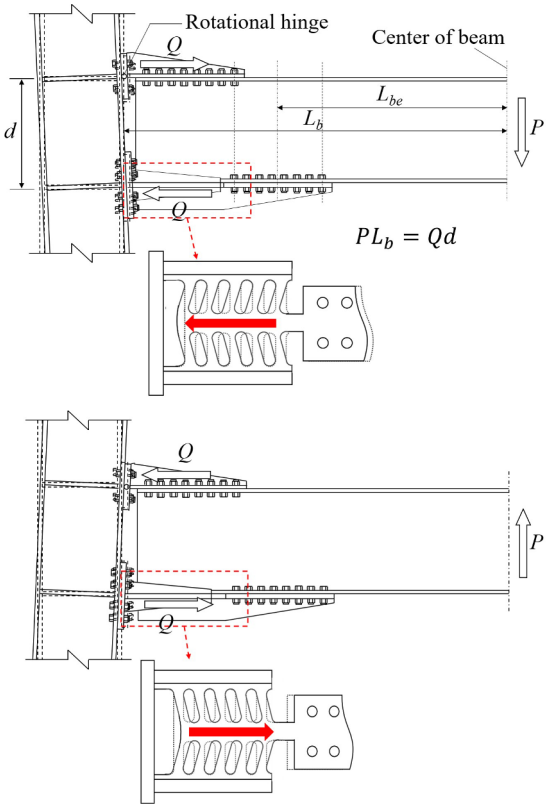

Fig. 2. Behavioral pattern of the proposed connection.

where k_{uf} and k_{lf} are the out-of-plane direction elastic stiffnesses of the upper and lower T-flanges, calculated as shown in Fig. 5. k_{us}, k_{ls1}, and k_{ls2} are the axial elastic stiffnesses (EA/L) of the non-yielding region of the upper T-stem and non-yielding regions 1 and 2 of the lower T-stem including each vertical rib, respectively, as defined in Fig. 6. I_b and A_{bw} are the moment of inertia for the strong axis of the beam and the cross-sectional area of the beam web. G is the shear modulus of the material. The axial elastic stiffness of the slit damper, k_d, can be expressed as follows using Eq. (2).

$$k_d = \frac{Q_{yd}}{\delta_{yd}} = \frac{nEtB}{1.5H_T}\left[\frac{1}{(H'/B)^2 + 2.6}\right] \tag{7}$$

The presented elastic stiffness formula evaluates the elements that have a dominant influence on the proposed connection detail in an approximate manner for the sake of simplification. In the case of out-of-plane direction elastic stiffness for T-flanges, the presented calculation method produces a somewhat conservative result because each of the upper and lower connectors has a vertical rib. This may compensate for

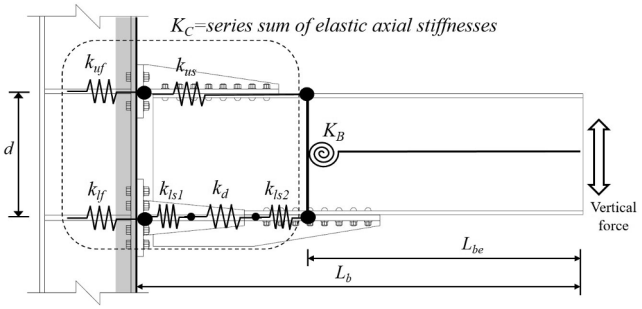

Fig. 4. Virtual elastic stiffness model.

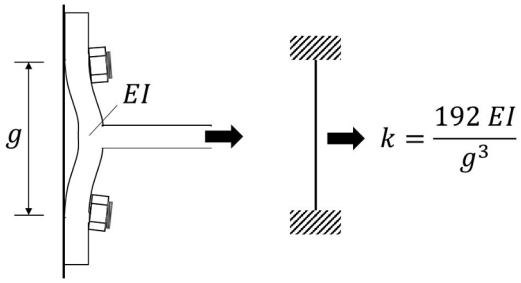

Fig. 5. Elastic axial stiffness contribution due to bending stiffness in T-flange.

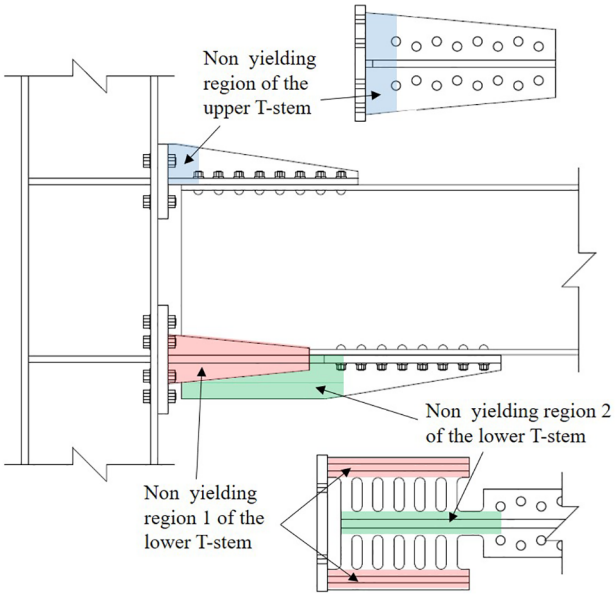

Fig. 6. Definition of non-yielding regions.

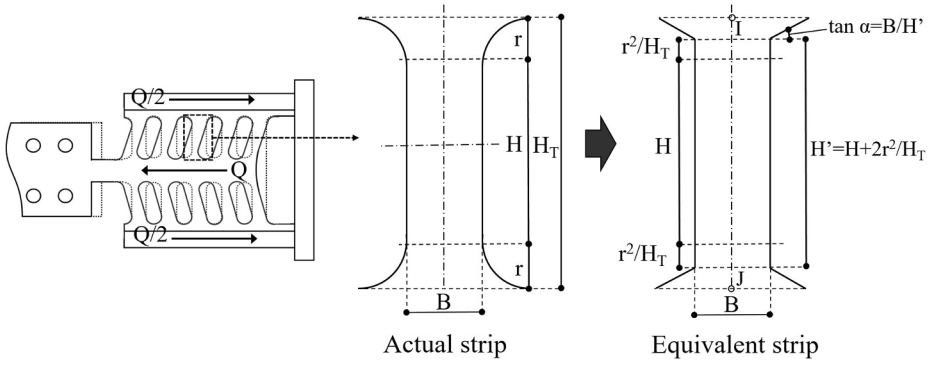

Fig. 3. Design parameters of the damper.

Table 1
Sectional properties of structural members.

Member type	Section	Manufacturing Method	Steel grade	I_x (cm^4)	Span (mm)
Beam	H-500 × 200 × 10 × 16	rolled shape	SS275 (Korean)	46,037	3,005
Column	H-400 × 400 × 13 × 21	rolled shape	SS275 (Korean)	65,362	3,000

the contribution of the regions not considered for the elastic stiffness, which were disregarded in order to simplify the formula. When the T-flange is sufficiently thick, and the bolt-fastening intervals are short, the influence of k_{uf} and k_{lf} on K_T is insignificant.

3. Experimental verification

3.1. Test specimens

A cyclic loading test was conducted to verify the structural performance of the TSD beam system. The shape of all specimens was set to the T-shaped beam-to-column connection. Table 1 lists the cross-sectional sizes and properties of the beam and column applied to all specimens. Both the beam and column were set to resist with strong axes. The relationship between the beam and column made of the same steel is compatible with the weak-beam mechanism. Fig. 7 shows the setting plan of the test.

The experimental variables were the damper/beam yield strength ratio, existence of a vertical rib in the upper T-stub, aspect ratio of the slit damper, and the difference in the attached area between the lower T-flange and lower T-stem. Table 2 lists the information on the experimental variables and Fig. 8 shows the details of the upper and lower connectors with an experimental variable. The damper/beam yield strength ratio, α, was classified into 0.4 and 0.6. When α is set to 0.6, the anticipated maximum moment of the beam system is expected to be similar to the full plastic moment of the beam with fully welded connection detail under the same conditions owing to the mechanical principle. Moreover, to identify the effect of the vertical rib of T-stub on the entire behavior of the connection, two out of the six specimens used typical T-stubs without a vertical rib and the rest four specimens used T-stubs with a vertical rib. The 6R1 and 6R2 specimens had the same length variables of the damper but were different in the connection detail between the lower T-flange and T-stem. 6R2 can be a more stable detail for the axial force generated in the connector compared to 6R1. The 6R3 and 6R4 specimens had different damper aspect ratios (H'/B) by adjusting the number of struts and the width of the damper even though they had the same damper design strength as the 6R2 specimen. In order to save steel volume, the connection of the upper and lower T-stem and the beam flange in all the specimens was applied with the staggered bolt pattern.

3.2. Boundary conditions and loading protocol

The beam and column were fastened with high-strength bolts to the upper and lower connectors. In particular, the beam and the upper and lower connectors were fastened as friction connections to prevent sliding in the shear connection. As shown in Fig. 7, for the boundary conditions, both ends of the column were connected to the steel jig with pin connections and forced displacement was applied to the free end of the beam through the hydraulic actuator. To prevent the lateral buckling of the beam during the test, lateral braces were installed at 1900 mm from the outer surface of the column toward the free end of the beam.

As a loading method, the beam-to-column connection cyclic loading procedure suggested by AISC 341 was used [17]. Considering the loading direction, the stroke direction of the actuator was set to the positive direction and the pulling direction was set to the negative direction. Negative loading was performed first during cyclic loading. Fig. 9 shows the test setup and loading protocol.

3.3. Measurement plan

The specimen was equipped with displacement transducers and strain gauges as shown in Fig. 10. Displacement transducers were installed at a total of 6 places including the same section at the opposite side of the loading point, one section (LVDT 2) for measuring the damper displacement, two sections (LVDT 3, 4) for the shear deformation of the panel, and another two sections (LVDT 5, 6) for the displacement measurement of column and panel. Strain gauges were attached to the damper expected as a plastic hinge, the end of the vertical rib, top and bottom beam flange, and the web considering the weak point of each element.

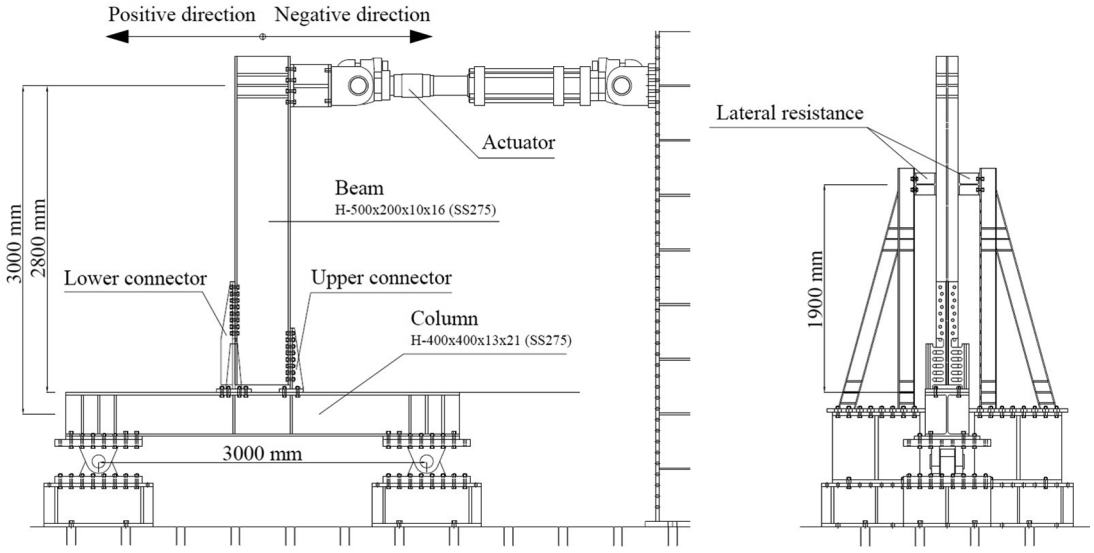

Fig. 7. Setting plan.

Table 2
Specimen information.

Specimen	T-stub type	Design damper/beam yield strength ratio, α	Number of strips, n	Length parameter (mm)			r (mm)	B (mm)	t (mm)	H′/B
				H	H′	H_T				
4NR	General	0.4	8	70	70.3	100	15	32	25	2.20
6NR	General	0.6	12	70	70.3	100	15	32	25	2.20
6R1	with vertical rib	0.6	12	70	70.3	100	15	32	25	2.20
6R2	with vertical rib	0.6	12	70	70.3	100	15	32	25	2.20
6R3	with vertical rib	0.6	16	70	70.3	100	15	28	25	2.51
6R4	with vertical rib	0.6	4	70	70.3	100	15	56	25	1.26

※ Specimen name : 6 R 1
: Design damper-to-beam yield strength ratio (4:0.4, 6:0.6)
: R: with vertical rib in T-stub; NR: no vertical rib in T-stub
: Classification according to shape of lower connector and aspect ratio of damper

3.4. Material properties

The beam, column, and upper and lower connectors of the specimens were made of the same steel grade (SS275, Korean). In the case of the damper, three T-stems were cut from each of the two steel plates (a: 4NR, 6NR, 6R1; b: 6R2, 6R3, 6R4). Coupon tests were conducted before the cyclic loading test. Table 3 lists the average values of three coupon tests on the main structural members. In the material tensile test results, the yield strength of the damper material was much higher than that of the beam material. Therefore, the actual damper/beam yield strength ratio of each specimen was relatively higher than the design value.

3.5. Overall test results

Fig. 11 shows moment-rotation curves. The moment and the rotation angle indicated in Fig. 11 were calculated by the load of the actuator multiplied by the length from the loading point to the column surface, and the displacement measured at the loading point divided by the length from the loading point to the center line of the column, respectively. And the ultimate states are shown in Fig. 12. For 6NR, i.e., the second specimen, the test was terminated because the lateral buckling of the beam occurred under the 0.03 rad 1 cycle loading due to the loose fastening of the bolts at the bottom of the lateral braces. Subsequently, sufficient fastening force was provided to prevent the

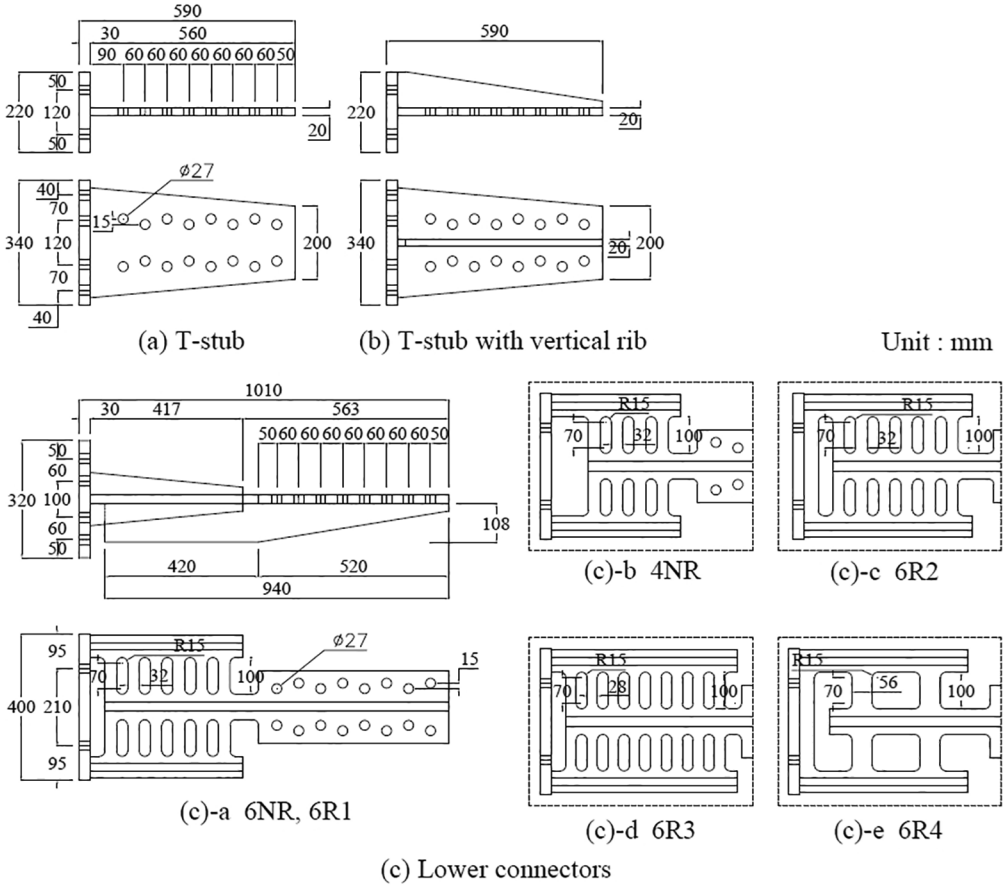

Fig. 8. Connector details.

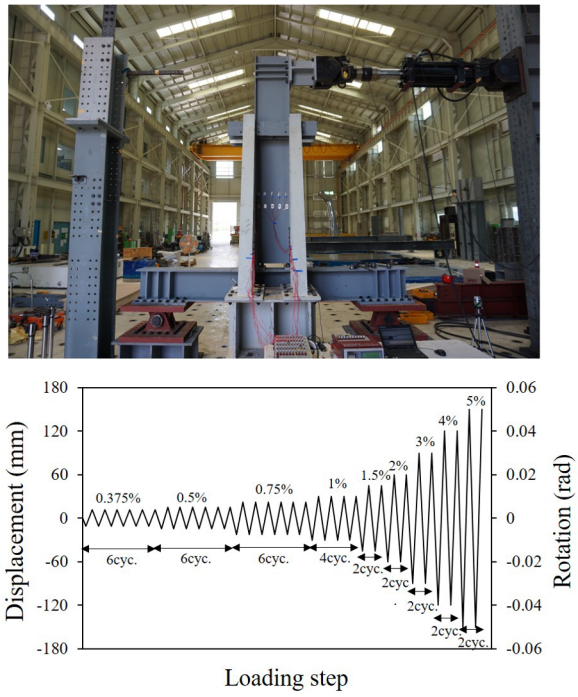

Fig. 9. Test setup (6R1) and loading protocol.

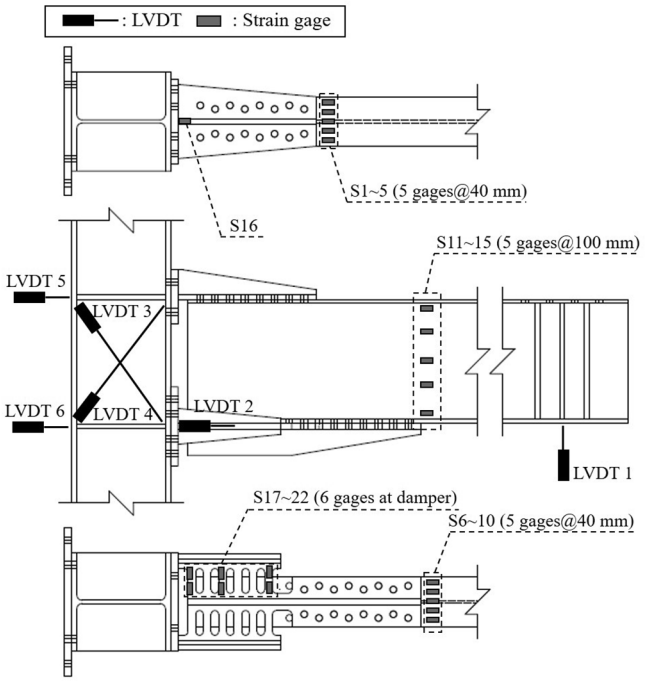

Fig. 10. Sensor installation plan.

Table 3
Average material properties of structural members from coupon tests.

Location	Young's modulus (MPa)	Yield stress, σ_y (MPa)	Ultimate stress, σ_u (MPa)	Elongation (%)	σ_y/σ_u
Beam	206,886	258.03	440.05	30.6	0.59
Column	214,023	313.93	458.89	29.3	0.68
Damper-a	190,565	290.37	418.82	29.9	0.69
Damper-b	199,741	303.28	460.96	30.4	0.65

same phenomenon. For the 6R4 specimen, the fracture of the damper occurred at 0.03 rad 2 cycle. Except for 6NR and 6R4, all specimens resisted the connection rotation angle of 0.04 rad. The test results showed that the failure mode led to damage in the damper for the all specimens. There was no evident damage to the beam or column. To derive the yielding point of each specimen, the skeleton curve was extracted from the hysteresis curve as shown in Fig. 13. A previous study [18] revealed that the skeleton curve derived using the method of Fig. 14(a) coincides with the M-θ relationship obtained from monotonic loading. For the extracted skeleton curves in the positive and negative loading, the yielding point was derived using the method of Fig. 14(b). Table 4 summarizes the main test results including the information on the yielding point. As evident from the M-θ relationship, the TSD beam system can guarantee similar strengths against loadings in the positive and negative direction through the same damper behavior and provide stable hysteretic behavior. The maximum moment of the 4NR specimen was approximately 80% of the full plastic moment of the beam while that of the specimens with a damper/beam yield strength ratio of 0.6 was higher than the M_p of the beam. In particular, 6R1, 6R2, and 6R3 met the required performance of the SMF in accordance with AISC.

4. Finite element analysis

4.1. Parameters and analysis method

Multivariate analysis was conducted to examine the structural performance according to the aspect ratio of the beam and damper/beam yield strength ratio. For the aspect ratio of the beam, the rolled H-beams of three cross-sections with height/width ratios of 2, 2.5, and 3 were selected as the analytical models considering the low- and middle-rise steel structures. The damper/beam yield strength ratio ranged from 0.2 to 1.6 with an interval of 0.2. As a comparison model, a full welded connection (FWC) model with a 1/4 circular weld access hole was added. Therefore, a total of 27 analytical models were constructed. Table 5 lists the information on the analytical models. The names of the analytical models were expressed using the beam height, connection detail, and damper/beam yield strength ratio. ANSYS was used as the analysis software [19]. The finite element model used SOLID 45 element, which has 24 nodal degrees of freedom and three translational DOFs at each node. To intensively observe the characteristics of the beam with TSD, the analytical models modeled only the upper and lower connectors and the beam. All TSD beam system analytical models had the same dimensions of the upper and lower connectors as those of the upper and lower connectors of 6R1, and only the damper thickness was adjusted according to the damper/beam yield strength ratio. The 6R1 specimen is a representative model with sufficient strength beyond the full plastic moment of the beam and having flexural yielding design about the damper. As shown in Fig. 15 (a), for the boundary conditions, the TSD model restrained the displacement of the T-flange and the FWC model restrained the displacement of the beam end in the x, y, and z directions. Sufficient forced displacement with a rotation angle of 0.05 rad or higher was applied to the free end of the beam in the upward direction. The contact boundary condition between the damper and lower flange of the beam in the TSD model prevented the penetration between the elements. In addition, a friction coefficient of 0.01 was provided. For monotonic analyses, multilinear isotropic hardening was used based on the material test results. The material properties were applied to all elements including the beam and connectors by replacing the relationship between the engineering stress and engineering strain in the results of the material tensile test on SS275 steel conducted by the author, shown in Table 6, with the relationship between the true stress (σ_t) and true strain (ε_t) by the following equation.

$$\sigma_t = \sigma_E(1+\varepsilon_E),\ \varepsilon_t = ln(1+\varepsilon_E) - \sigma_E/E \quad (8)$$

In addition to the abovementioned analytical models, an analytical model was constructed to secure the reliability of the FEA results. The

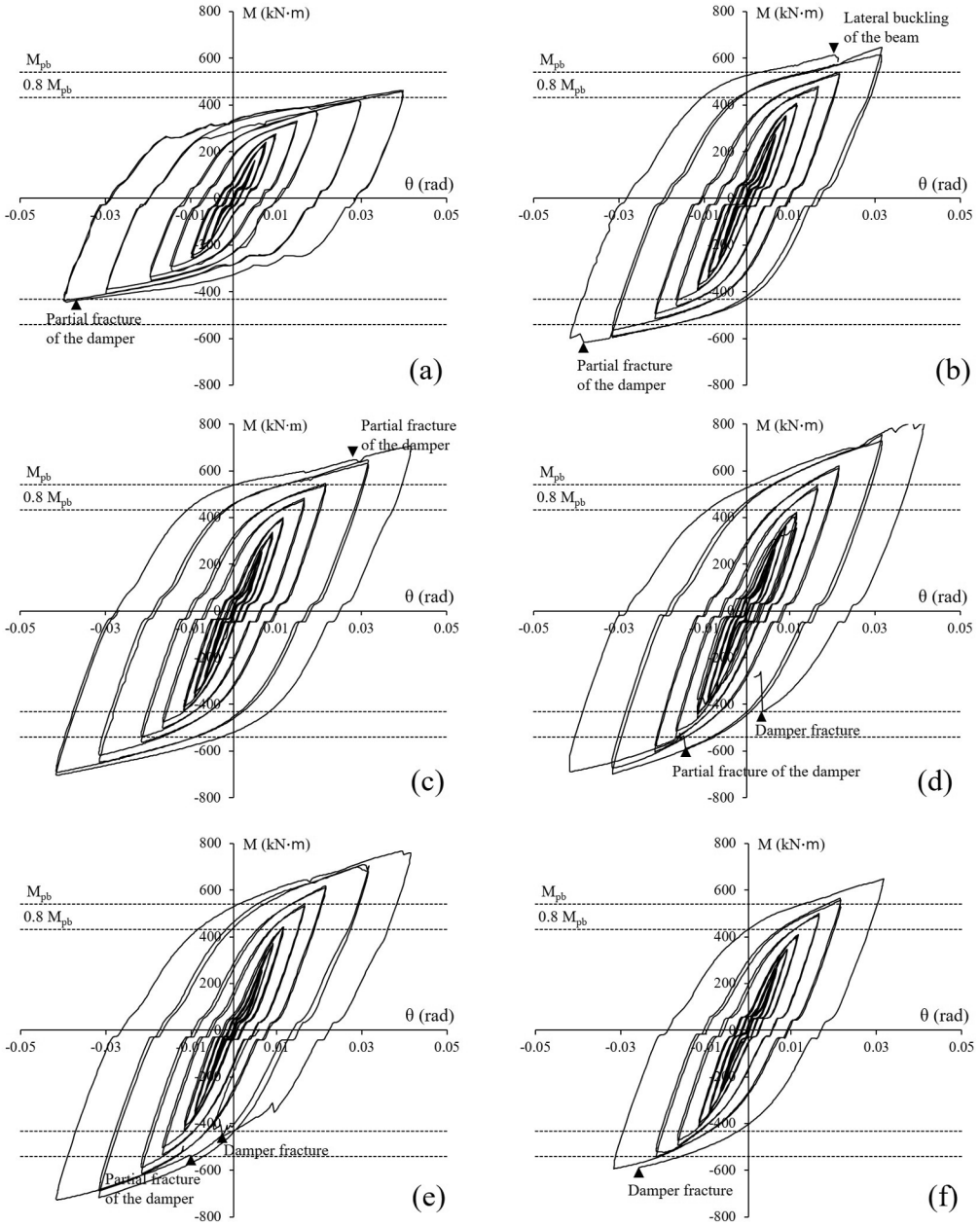

Fig. 11. Moment-rotation curves: (a) 4NR, (b) 6NR, (c) 6R1, (d) 6R2, (e) 6R3, and (f) 6R4.

reliability verification model had the same dimensions and boundary conditions as 6R1, as shown in Fig. 15(c). The material test results summarized in Table 3 were replaced with the true stress–true strain relationship and applied to each element.

4.2. Comparison with test results

Fig. 16 compares the FEA results of the reliability verification model with the test results. In Fig. 16(a), the monotonic hysteresis curve of the FEA is compared with the skeleton curve of 6R1 under negative direction loading. The monotonic hysteresis curve exhibits a slightly higher initial stiffness than the test results; however, the overall load history trend is similar to the test results. Moreover, Fig. 16(b) shows that the deformation of the damper was dominant owing to the occurrence of forced displacement of the connection. Therefore, it appears that the analytical model can effectively reflect the design intent of the proposed connection detail and provide reliable results data.

4.3. Overall FEA results

Table 7 and Fig. 17 present the main results of the multivariate analysis and moment-rotation relationship. Fig. 18 shows the PEEQ contour of the 500 series analytical models at a rotation angle of 0.04 rad. The plastic deformation of the FWC model was concentrated on the weld access hole and the edge of the flange at the beam end. Earthquake experience in the past [20,21] confirmed that such damage concentration on heat affected zone is the major cause of the brittle fracture at the beam end. In the TSD model, however, plastic deformation occurred in the upper T-stub and slit damper at relatively lower damper/beam yield strength ratios and the beam member exhibited elasticity-like behavior over the entire area as shown in Fig. 18. As the damper/beam yield strength ratio increased, the sharing of the deformation by the damper decreased for the same connection deformation, and obvious plastic deformation was confirmed at the effective length of the beam when the damper/beam yield strength ratio

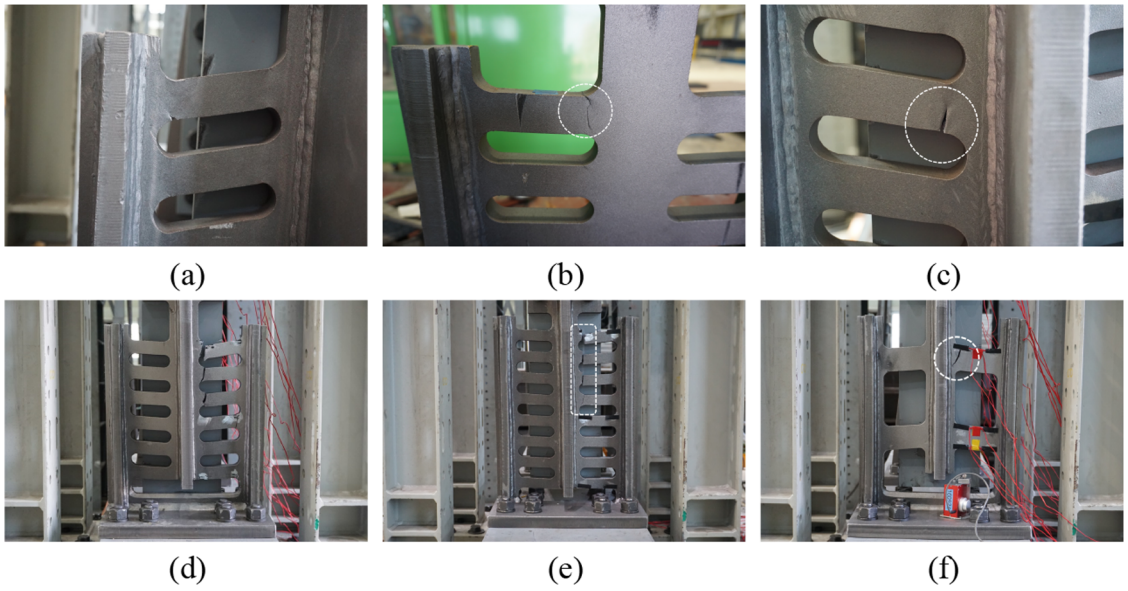

Fig. 12. Damper situations at ultimate state: (a) 4NR, (b) 6NR, (c) 6R1, (d) 6R2, (e) 6R3, (f) 6R4.

was 1.2 or higher. In Table 7, the maximum moment in the analysis, M_m, is considered the moment at the rotation angle of 0.04 rad. Accordingly, the ratio of maximum moment to the yield moment, M_m/M_y, exhibited a value of approximately 1.2 for the FWC model. The M_m/M_y of the TSD models decreased from approximately two to 1.2 as the damper strength increased. This is because the behavior of the beam gradually dominated the overall behavior of the system. After the point where the TSD beam system simulated the behavior of a haunched beam, the yield moment and maximum moment converged to specific values.

5. Discussion

5.1. Strength evaluation

Fig. 19 shows the yield strength ratio obtained in the test and FEA based on the designed damper/beam yield strength ratio (α). The vertical axis of Fig. 19 represents the ratio of the yield moment of the TSD model to that of the FWC model in the FEA and the ratio of the yield moment of the specimen to that of the beam ($M_{yb} = \sigma_{yb}S_x$) obtained in the coupon test results. The yield moment obtained in the test and FEA was slightly higher than the approximation values when the value of α varied between 0.8 and 1.4, but it generally exhibited similar responses.

Fig. 20 shows the ratio of the maximum moment to the full plastic moment of the beam, M_{pb}, according to α. The horizontal red dotted lines in Fig. 20 represent the ratio of the beam span to effective length of the beam (L_{be}), implying that the level at which the moment of the beam at the end of the effective length reached the full plastic moment. The FEA results showed that the maximum moment converged to approximately 120% of the full plastic moment of the beam considering the effective length as α increased. In this case, the failure mode of the connection is determined by the ultimate state of the beam, as shown in Fig. 18. As presented in Table 7, the maximum strength was observed when the value of α was set between 0.6 and 0.7, which was equivalent to that of the FWC model. It was found that the value of α should be approximately between 0.5 and 0.6 to be consistent with M_{pb} according to the mechanical equation. The maximum moment of the TSD beam system designed with a lower yield moment than that of the beam ($\alpha \leq 1$) could meet M_{pb}. This is because the yielding of TSD beam system to the maximum moment dominated by the structural characteristics of the slit damper was higher than that of typical flexural members. In Table 4, M_m/M_y from the test results ranged from 1.7 to two. In addition, as summarized in Table 7, M_m/M_y was approximately 1.5 when α was one. However, as the value of α increased, the value of M_m/M_y converged to 1.2, which is the value for typical flexural members. This relatively larger margin for strength easily induces the

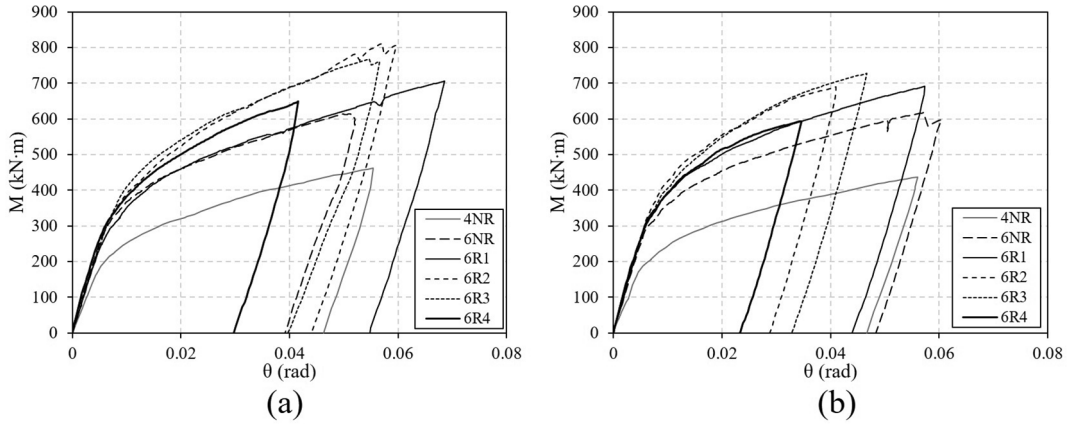

Fig. 13. Skeleton curve: (a) positive loading and (b) negative loading.

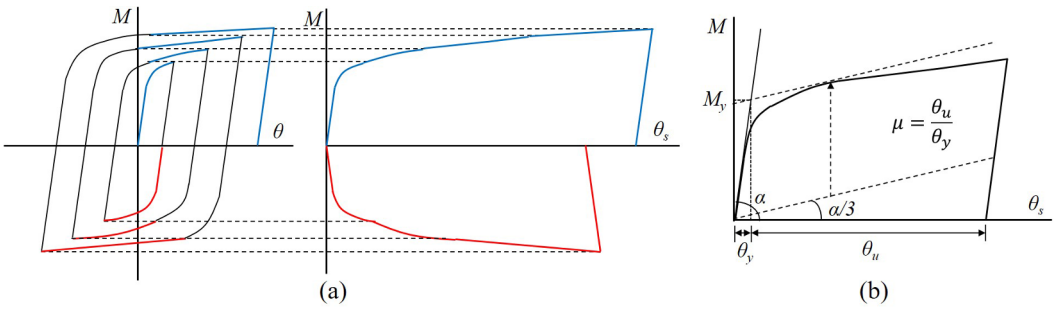

Fig. 14. Derivation of yielding point: (a) concept of skeleton curve and (b) yielding point and ductility.

Table 4
Test results.

Specimen	Actual damper-beam strength ratio	Direction loading	Elastic stiffness (N/mm)	M_y (kN m)	M_m (kN m)	M_m/M_y	M_y/M_{yb}	M_m/M_{pb}	μ
4-NR	0.444	Positive	5233	222.50	461.78	2.08	0.47	0.85	9.11
		Negative	5592	217.35	443.69	2.04	0.46	0.82	9.75
6-NR	0.668	Positive	6370	330.64	645.65	1.95	0.70	1.19	6.82
		Negative	6729	322.07	617.29	1.92	0.68	1.14	9.11
6-R-a	0.668	Positive	6233	323.51	706.69	2.18	0.68	1.31	9.55
		Negative	7031	353.56	704.67	1.99	0.74	1.30	7.89
6-R-b	0.720	Positive	6486	380.30	811.47	2.13	0.80	1.50	6.79
		Negative	6578	395.63	698.30	1.77	0.83	1.29	4.81
6-R-c	0.735	Positive	6366	398.24	747.42	1.88	0.84	1.38	6.34
		Negative	7031	379.85	727.66	1.92	0.80	1.35	5.49
6-R-d	0.735	Positive	6981	341.83	648.42	1.90	0.72	1.20	5.17
		Negative	7186	349.44	593.76	1.70	0.74	1.10	4.08

M_{yb}, M_{pb} are the theoretical yield moment and full plastic moment of the beam member, respectively.

Table 5
Classification of analytical models.

Model name	Beam section	Beam shape ratio, H/B	Connection detail	Damper-to-Beam yield strength ratio
404/FWC	H-404 × 201 × 9 × 15 (404 series)	2.01	full welded connection	–
404/TSD/0.2~1.6			TSD system	0.2–1.6 (interval: 0.2)
500/FWC	H-500 × 200 × 10 × 16 (500 series)	2.50	full welded connection	–
500/TSD/0.2~1.6			TSD system	0.2–1.6 (interval: 0.2)
600/FWC	H-600 × 200 × 11 × 17 (600 series)	3.00	full welded connection	–
600/TSD/0.2~1.6			TSD system	0.2–1.6 (interval: 0.2)

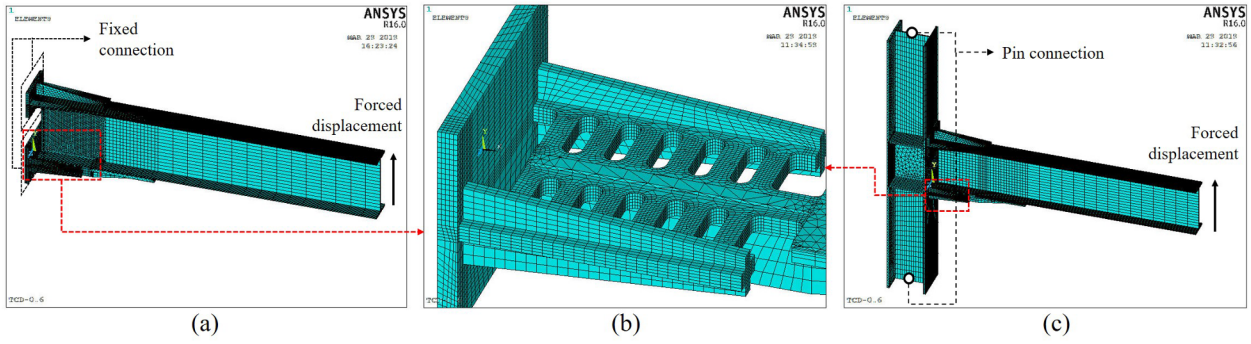

Fig. 15. Mesh models: (a) main model, (b) slit damper part, and (c) reliability verification model.

Table 6
Material properties for FEA.

Steel grade	Young's modulus (MPa)	Yield stress, σ_y (MPa)	Ultimate stress, σ_u (MPa)	σ_y/σ_u
SS275	197,235	284.12	420.16	0.68

preceding yielding of a specific connection element and provides the benefit of securing the required strength of the connection in terms of design. However, when a large deformation occurs in the connection, the maximum strength of the beam system become greater than the required strength value, which may result in a weak column. Therefore, an appropriate design damper/beam strength ratio that meets the design requirements must be selected.

The upper T-stub constituting the TSD connector has a vertical rib. Stress concentration may occur at the end of the vertical rib depending

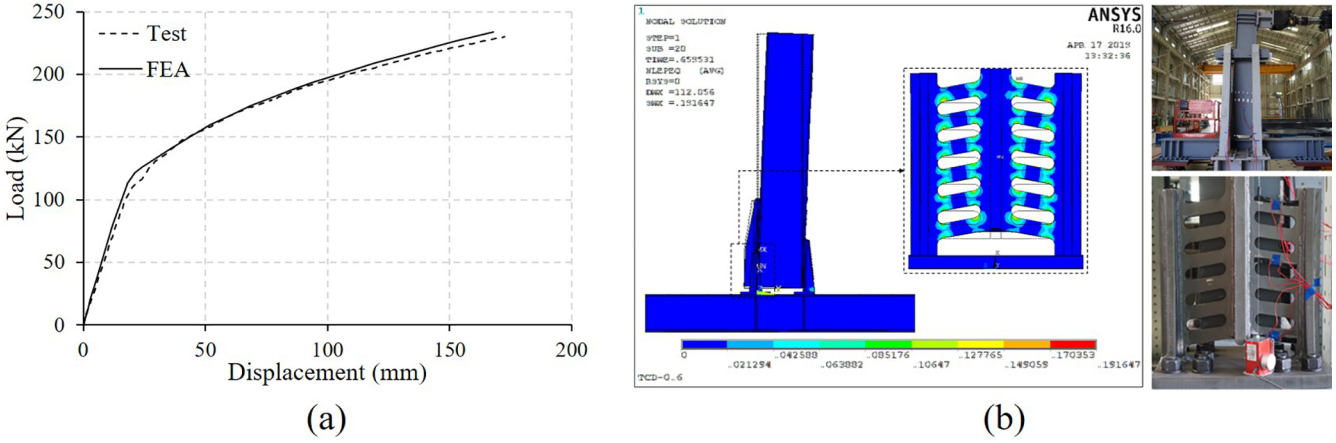

Fig. 16. Comparison between FEA results and test results: (a) load-displacement curve and (b) PEEQ contour and test ultimate state at a rotation angle of 0.04 rad.

Table 7
FEA results.

Model name	α	Elastic stiffness (N/mm)	M_y (kN m)	M_m (kN m)	M_m/M_y	$M_y/M_{y,FWC}$	$M_m/M_{m,FWC}$
404/FWC	–	6457	410.33	489.70	1.19	1.00	1.00
404/TSD/0.2	0.2	4253	98.36	195.17	1.98	0.24	0.40
404/TSD/0.4	0.4	6374	178.76	341.38	1.91	0.44	0.70
404/TSD/0.6	0.6	7351	275.84	473.41	1.72	0.67	0.97
404/TSD/0.8	0.8	8460	374.80	619.58	1.65	0.91	1.27
404/TSD/1.0	1.0	8942	473.54	713.97	1.51	1.15	1.46
404/TSD/1.2	1.2	9588	570.79	749.36	1.31	1.39	1.53
404/TSD/1.4	1.4	10,019	640.55	767.14	1.20	1.56	1.57
404/TSD/1.6	1.6	10,437	648.15	800.18	1.23	1.58	1.63
500/FWC	–	10,927	577.45	709.27	1.23	1.00	1.00
500/TSD/0.2	0.2	7242	123.97	263.62	2.13	0.21	0.37
500/TSD/0.4	0.4	10,117	249.34	474.61	1.90	0.43	0.67
500/TSD/0.6	0.6	12,259	361.64	663.90	1.84	0.63	0.94
500/TSD/0.8	0.8	13,575	524.19	873.27	1.67	0.91	1.23
500/TSD/1.0	1.0	14,838	654.12	1006.93	1.54	1.13	1.42
500/TSD/1.2	1.2	15,744	788.12	1072.53	1.36	1.36	1.51
500/TSD/1.4	1.4	16,287	888.63	1119.36	1.26	1.54	1.58
500/TSD/1.6	1.6	17,111	920.79	1061.75	1.15	1.59	1.50
600/FWC	–	17,062	787.63	989.86	1.26	1.00	1.00
600/TSD/0.2	0.2	11,279	151.14	348.89	2.31	0.19	0.35
600/TSD/0.4	0.4	15,899	308.32	638.30	2.07	0.39	0.64
600/TSD/0.6	0.6	18,520	472.44	901.01	1.91	0.60	0.91
600/TSD/0.8	0.8	20,861	640.84	1154.55	1.80	0.81	1.17
600/TSD/1.0	1.0	22,175	825.50	1355.65	1.64	1.05	1.37
600/TSD/1.2	1.2	23,752	991.11	1447.69	1.46	1.26	1.46
600/TSD/1.4	1.4	24,036	1138.50	1500.88	1.32	1.45	1.52
600/TSD/1.6	1.6	25,340	1217.84	1551.62	1.27	1.55	1.57

Maximum moment of FEA results, M_m, is the moment at 0.04 rad of the rotation of the beam system.

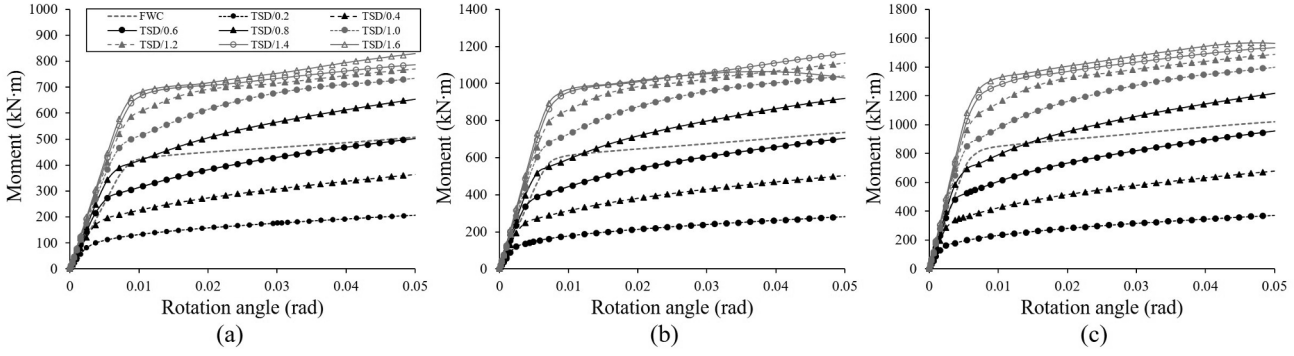

Fig. 17. Moment-rotation according to FEA results: (a) 404 series, (b) 500 series, and (c) 600 series.

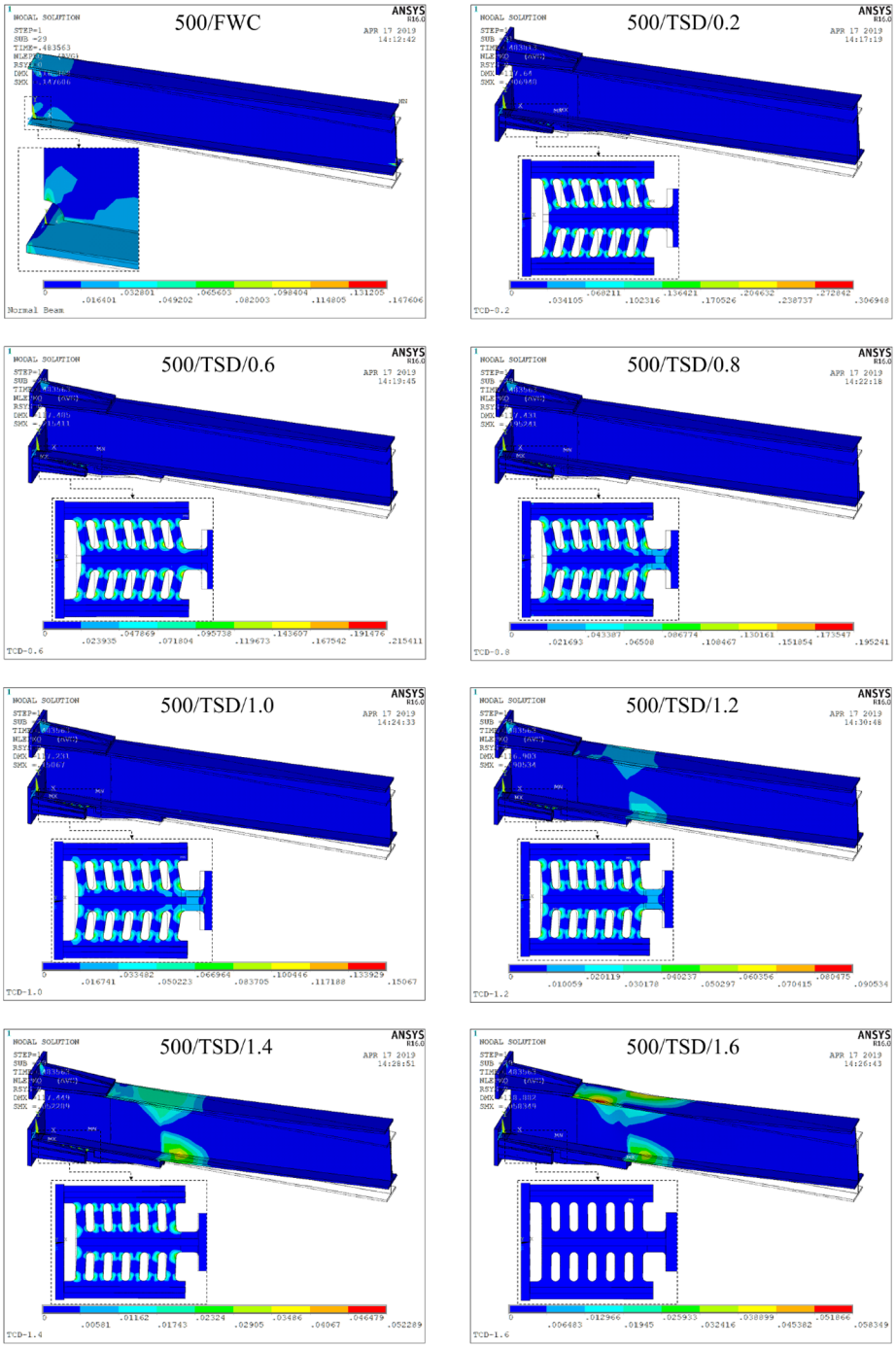

Fig. 18. PEEQ contour at a rotation of 0.04 rad about 500 series models.

on the rotational deformation of the connection. In the design concept, the upper T-stem was assumed to act as a neutral axis. The failure mode and strength contribution of the vertical rib were not considered. To examine these, the strain of the damper was compared with that of the vertical rib, as shown in Fig. 21. Moreover, the maximum moment values at each loading step of 6NR and 6R1, which had the same condition except for the vertical rib, were compared, as shown in Fig. 22. The behavior of the vertical rib in response to cyclic loading exhibited a larger deformation in the compression zone than in the tensile zone. Yielding began at a rotation angle of approximately 0.02 rad. The overall strain magnitude was considerably smaller than that of the damper. The maximum strength of 6R1, according to the connection rotation, was similar to that of 6NR under positive loading. However, approximately 10% overstrength occurred under negative loading. This coincides with the results of Fig. 21 where a greater deformation occurred in the compression directions. In summary, the vertical rib of the T-stub resulted in an additional difference in the compression zone with respect to the T-stem, which was the rotation axis, but did not considerably contribute to the strength of the entire connection system.

5.2. *Effect of aspect ratio of damper*

The flexural yielding condition of the slit damper applied to the proposed connection detail can be expressed using the effective length of the damper, H', and the width of the damper, B, as follows [22].

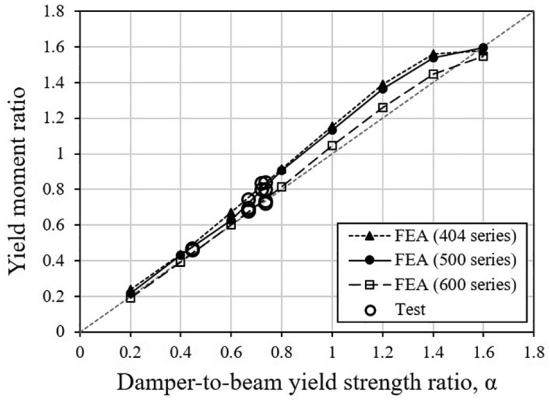

Fig. 19. Yield moment ratio according to α.

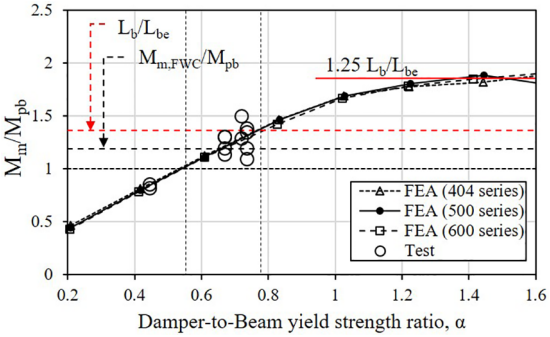

Fig. 20. Maximum moment ratio according to α.

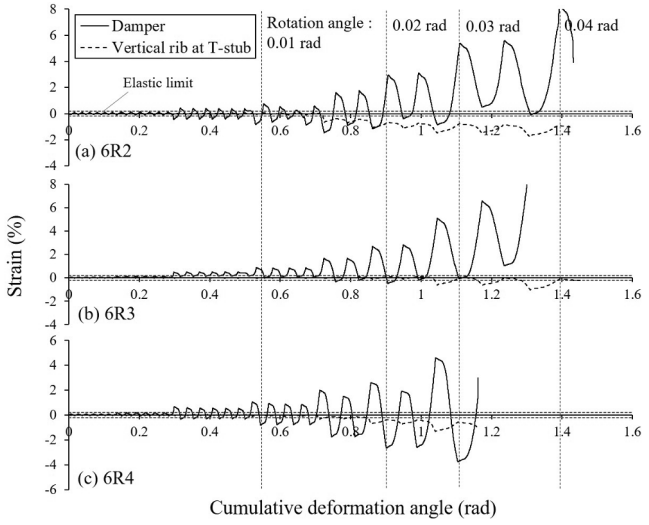

Fig. 21. Comparing strain history of the damper and vertical rib.

$$H'/B > 3\sqrt{3}/4 \quad (9)$$

Based on the conditions set in the test plan, the dampers of 4NR, 6NR, 6R1, and 6R2 had an H′/B value of 2.2, and the damper of 6R3 had an H'/B value of 2.51. They were designed as flexural yielding types. However, the H'/B of the damper of 6R4 was designed to be 1.26, and it had an aspect ratio close to the shear yielding mechanism. In the test results, the average ductility ratio (μ) of 6R4 was less than five, and the specimen exhibited a lower ductility than other specimens. As the structural performance of the TSD beam system directly depends on the performance of the damper in the design concept, the design must allow the damper to exhibit sufficient flexural yielding behavior. However,

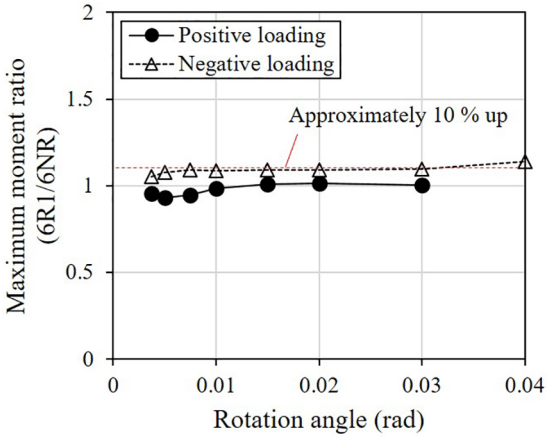

Fig. 22. Increase in strength according to vertical rib installation.

6R3 with a higher H'/B value did not exhibit better ductility than the specimen with an H'/B value of 2.2.

5.3. Damage distribution and damper design range consideration

In the test results, the rotational deformation of the connection is expressed as the sum of the deformations in the beam, column, panel zone, and damper. Fig. 23 shows the load-displacement relationships of each component of the main specimens obtained from the measured sensor responses. Fig. 24 compares the energy absorbed by each component according to the load-displacement relationship. Owing to the damper/beam yield strength ratios set in the test, the deformation of the connection was concentrated on the damper throughout the loading. The damper absorbed approximately 90% of the total energy of the connection. The hysteretic behavior of the beam, column, and panel exhibited hysteresis loops close to elastic behavior but their hysteretic behavior in the test results included the smaller areas. Fig. 25 shows the strain profiles at the damper and the beam of the representative specimen of 6R1. All specimens exhibited similar strain profiles. Regarding the strength relationship between the beam and the damper, which constitute the TSD beam system, the damper yielded earlier owing to its positional characteristics. However, as the margin of the maximum strength to the yield strength of the damper (σ_{ud}/σ_{yd}) is relatively large, the yielding and ultimate state of the beam may occur while the damper reaches the ultimate state. Fig. 26 shows the beam maximum strain distributions of the specimens according to the connection rotation. It was confirmed that the beam that exhibited elastic behavior up to a rotation angle of 0.02 rad, while plastic deformation occurred at 0.03 rad or higher. Obviously, such damage to the beam will increase as α increases. Fig. 27 displays the FEA results of the PEEQ index of the damper according to α. The PEEQ index is the damage index for plastic behavior, expressed as the ratio of the equivalent plastic strain (PEEQ) to the yield strain (ε_y) [23]. Fig. 28 shows the ratio of the yield strain to the maximum strain of the beam and the ratio of the maximum moment to the full plastic moment of the beam according to the damper/beam yield strength ratio. When the moment frame is constructed for damage control, improved structural performance can be obtained as the strain ratio and moment ratio of the beam increase. For the damper/beam yield strength ratios set in the analysis, the damper involved plastic deformation in all analytical models. The magnitude of plastic deformation of the damper was inversely proportional to the increase in α. The plasticity of the beam, however, increases as α increases. Therefore, $\varepsilon_{yb}/\varepsilon_b$ and M_m/M_{pb} have limited design ranges depending on the required structural goals. For example, a damper/beam yield strength ratio of approximately 0.5 can be recommended to maintain the elasticity of the beam and secure a strength higher than the full plastic moment even under sufficient deformation of the connection.

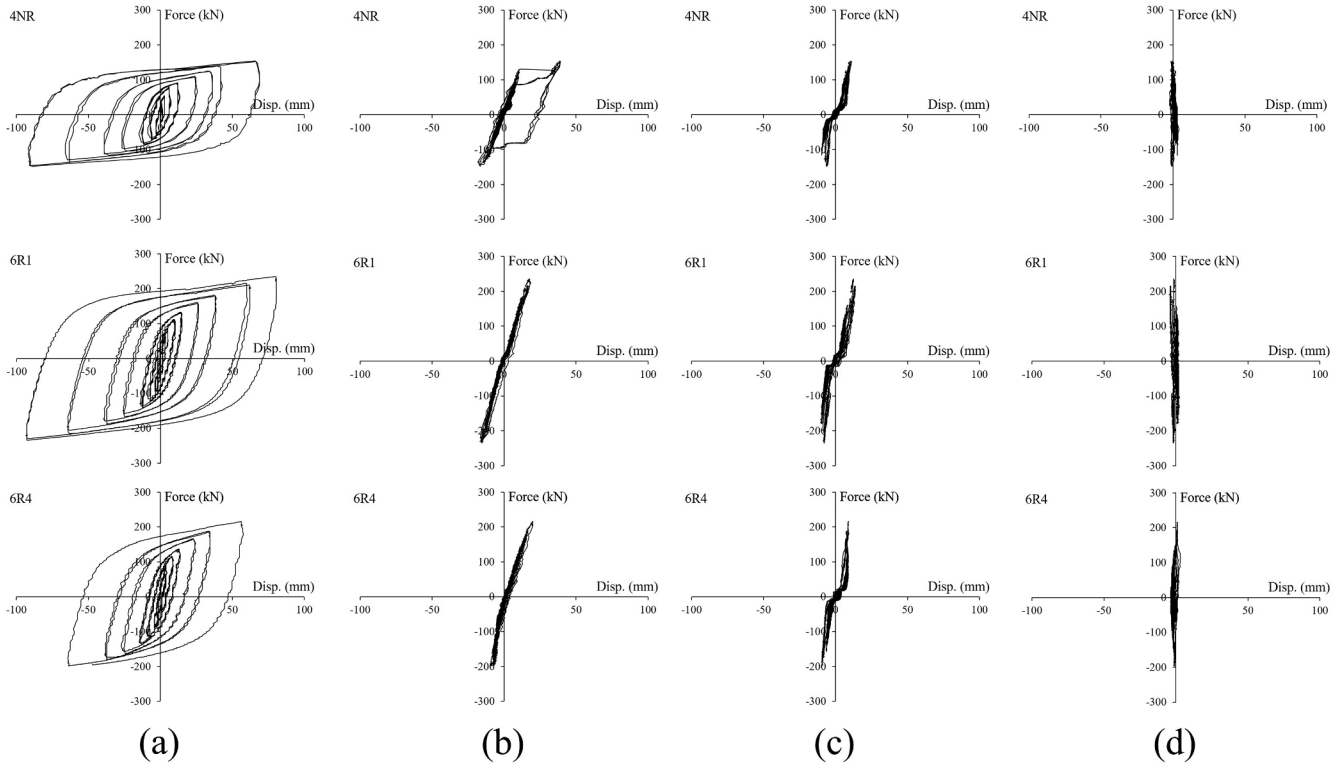

Fig. 23. Hysteresis loops of connection components: (a) damper, (b) beam, (c) column, and (d) panel.

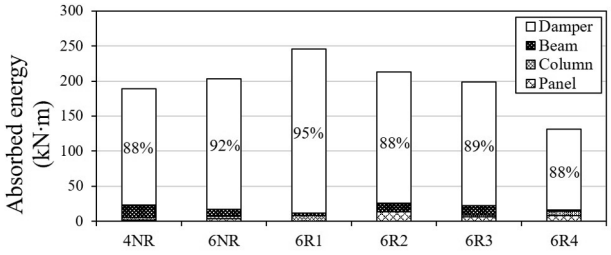

Fig. 24. Absorbed energy distribution according to components.

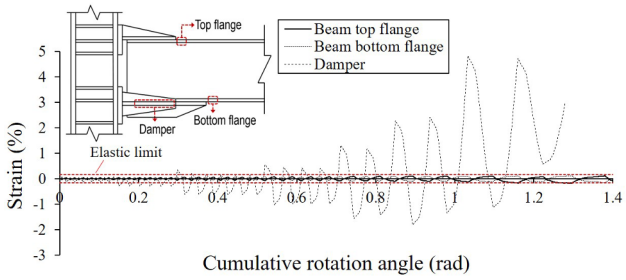

Fig. 25. Strain profiles at beam and damper of 6R1.

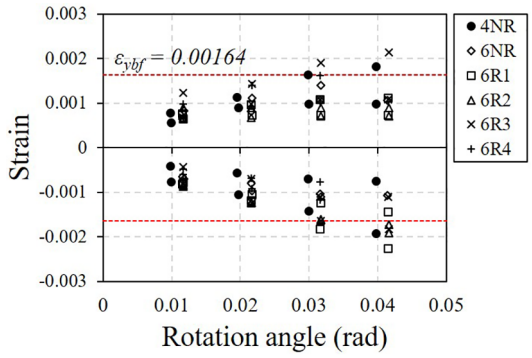

Fig. 26. Beam maximum strain distribution according to rotation angle.

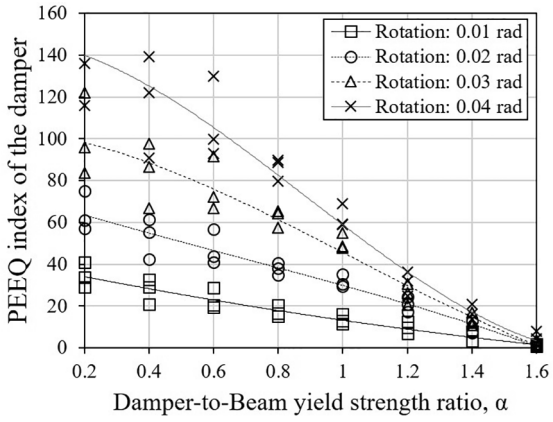

Fig. 27. PEEQ index of damper according to α.

When the yield strength of the damper is equal to that of the beam, the beam system can secure a strength higher than M_{pb} after yielding, with the damper involving sufficient inelastic behavior. In this case, however, the beam member also involves plastic deformation such that $\varepsilon_{yb}/\varepsilon_b = 0.5$. For the sufficient plastic deformation of the damper and the weak-beam mechanism, a damper/beam yield strength ratio of one or greater is not recommended. As the results of this study were obtained from general beam member sizes that can be used in low- and mid-rise steel structures, the performance curve shown in Fig. 28 can provide reasonable damper design ranges of the damper for similar environments. The performance curve of $\varepsilon_{yb}/\varepsilon_b$, however, slightly changes according to the shift in the moment gradient as L_{be}/L_b changes over the beam span and installation length of the connector. Therefore, the design ranges must be verified in actual applications.

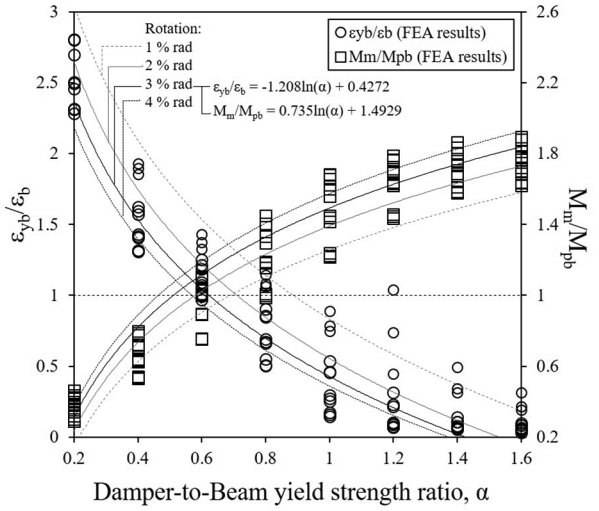

Fig. 28. Performance curve of beam damage and strength of beam system relationships according to α.

5.4. Elastic stiffness evaluation

Table 8 compares the elastic stiffness values between the test results and the predicted values. The values from the test results represent the elastic stiffness under positive loading while the values in parentheses indicate the elastic stiffness under negative loading. In all test results, the elastic stiffness under positive loading was lower than that under negative loading because the small out-of-plane direction deformation of the beam contributed to the stiffness in the connection even though support elements to prevent lateral buckling were installed. The 4NR specimen exhibited the largest error (16.6%) between the test value and the predicted value. However, in general, errors less than 10% were observed. Moreover, the FEA results were similar to the predicted values according to α, as shown in Fig. 29.

In FEMA-355D [24], the double angle connection detail and T-stub connection detail are classified as partially restrained (PR) construction. The PR connection detail must verify that the structural performance is satisfactory through physical verification and analytical results depending on the application situation. Fig. 30 compares the M-θ relationships from the test and FEA results with the conditions to secure the connection stiffness specified in AISC 360 [25]. The diagonal dotted lines in the graphs represent the stiffness corresponding to a fully restrained (FR) connection ($K_{FR} = 20EI_b/L$) and a simple connection ($K_S = 2EI_b/L$) level, respectively. EI_b and L denote the stiffness characteristic value of the beam and the beam length of one span, respectively. In the test results, the elastic stiffness of the TSD beam system exhibited PR connection level at α = 0.4, and values close to the FR connection at α = 0.6. According to the FEA results, the elastic stiffness of the TSD beam system at α = 0.8 or higher exceeds that of the full welded connection model. Considering the above results, it is expected that the TSD beam system can be designed in the FR connection and PR connection ranges by using the elastic stiffness formula and the hysteretic model to be mentioned in following section depending on the service load and the design intent.

5.5. Hysteretic model for TSD beam system

The hysteretic behavior of the TSD beam system depends on the structural behavior of the slit damper, according to the design concept. Fig. 31 shows the well-known hysteretic properties of the slit damper. Owing to the acting slit damper, the hysteretic model of the TSD beam system can be expressed as shown in Fig. 32. The initial stiffness in Fig. 32, K1, is obtained using Eq. (4). If the anticipated maximum strength of the system, M_{rbs}, occurs in the elastic region of the beam, i.e.

Table 8
Elastic stiffness evaluation according to test results.

Specimen	Elastic stiffness by formula (kN/m)										Test result, + (−) (kN/m)		Error (%)
	k_{tf}	k_{bf}	k_{tw}	k_{bw1}	k_{bw2}	k_d	$K_{con.}$	K_{beam}	K_{bs}	$K_{col.}$	K_T		
4NR	2.06×10^7	2.28×10^6	3.74×10^6	3.47×10^6	2.35×10^6	1.09×10^6	1.45×10^4	2.61×10^4	9329.72	19167.39	6275.247	5533(5592)	16.6(10.9)
6NR	2.06×10^7	2.28×10^6	3.74×10^6	2.92×10^6	1.74×10^6	1.64×10^6	1.52×10^4	2.83×10^4	9867.02	19167.39	6513.823	6370(6729)	2.2(3.3)
6R1	2.06×10^7	2.28×10^6	1.21×10^7	2.92×10^6	1.74×10^6	1.64×10^6	1.65×10^4	2.83×10^4	10414.69	19167.39	6748.087	6233(7031)	7.6(4.2)
6R2	2.06×10^7	2.28×10^6	1.21×10^7	2.92×10^6	1.67×10^6	1.64×10^6	1.63×10^4	2.94×10^4	10488.52	19167.39	6779.005	6486(6578)	4.3(3.0)
6R3	2.06×10^7	2.28×10^6	1.21×10^7	2.37×10^6	1.55×10^6	1.60×10^6	1.53×10^4	2.94×10^4	10046.58	19167.39	6591.596	6366(7031)	3.4(6.7)
6R4	2.06×10^7	2.28×10^6	1.21×10^7	3.23×10^6	1.85×10^6	1.70×10^6	1.72×10^4	2.94×10^4	10857.78	19167.39	6931.361	6981(7186)	0.7(3.7)

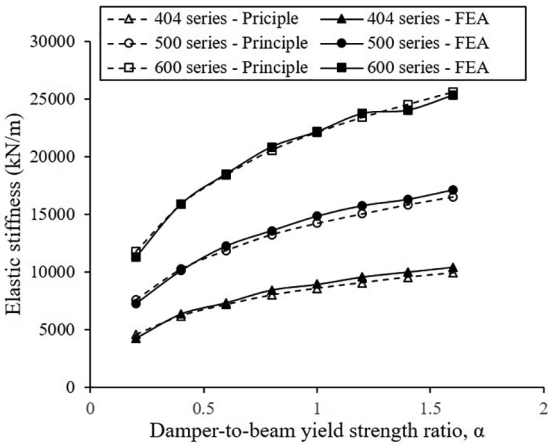

Fig. 29. Comparison between FEA results and approximated values for elastic stiffness.

under the condition of $M_{rbs} \leq (L_b/L_{be})M_{yb}$, the second and third stiffnesses after the system yields become the recalculated K_T when the horizontal stiffness of the damper, k_d, becomes $k_d/25$ and $k_d/125$, respectively, based on M_{ybs} and M_{rbs}. The yielding point of the beam can be classified into three cases, as shown in Fig. 32. Path (1) is the case where the yielding of the beam occurs at the end of the effective length prior to or simultaneously with the yielding of the damper. After yielding, the stiffness of the beam system becomes the recalculated stiffness of the entire system, reflecting the second stiffness of the flexural member. In this study, the second stiffness of general flexural member was set to 1/50th of the initial stiffness based on the results of previous study [26]. Path (1), however, is not the case considered in the design concept of the TSD beam system. When M_{ybs} is obtained from the yielding of the slit damper, the anticipated maximum strength of the beam system is expressed as $(\sigma_{ud}/\sigma_{yd})M_{ybs}$. In this case, the moment at which the beam yields is $[L_b/(\alpha L_{be})]M_{ybs}$. Therefore, paths (2) and (3) are determined based on the relationship between the yield ratio of the damper material, σ_{yd}/σ_{ud} and $\alpha(L_{be}/L_b)$. Similarly, based on the initiation of yielding of the beam, the subsequent stiffness becomes the stiffness, recalculated by applying $K_B/50$ to the stiffness of the previous step as K_B. In conclusion, the hysteretic properties of the TSD beam system are expressed using the third or fourth straight line depending on the presented elastic stiffness formula. For the beam yielding condition (3), the change in stiffness of the system due to the yielding of the beam is relatively insignificant, and the hysteretic properties of the entire system can be expressed through an approximation of a tri-linear model. As shown in Fig. 33, the proposed hysteretic model exhibits similar responses to the test and FEA results and can effectively represent the hysteretic properties of the TSD beam system.

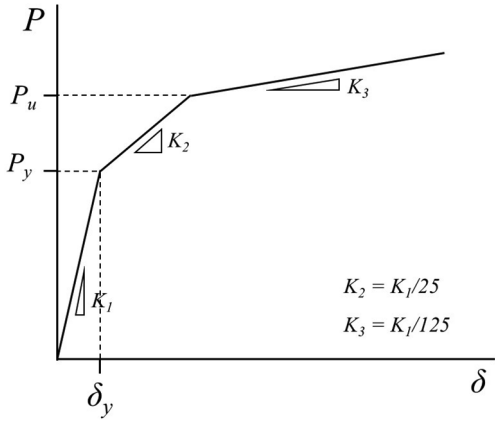

Fig. 31. Hysteretic properties of the steel slit damper.

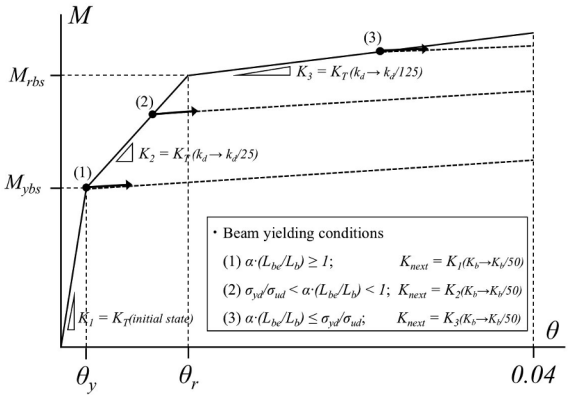

Fig. 32. Hysteretic model for the TSD beam system.

6. Conclusion

In this study, a new connection detail was proposed for the T-stub connection-type damage-controlled system. The proposed connection detail includes the upper and lower connectors that fasten the beam and column using bolts. The upper connector is a general T-stub having a vertical rib, and the lower connector contains a horizontally arranged steel slit damper as the energy absorption device. The proposed connection detail (TSD system) is a moment-resistance connection detail that can complement the existing detail by providing the same bidirectional resistance for the rotational behavior of the connection. This helps establish smooth flexure and shear behavior of the slit damper. The strength and stiffness formulas of the beam system with TSD were proposed according to the mechanical behavior characteristics of the connection. To practically verify them, a cyclic loading test was

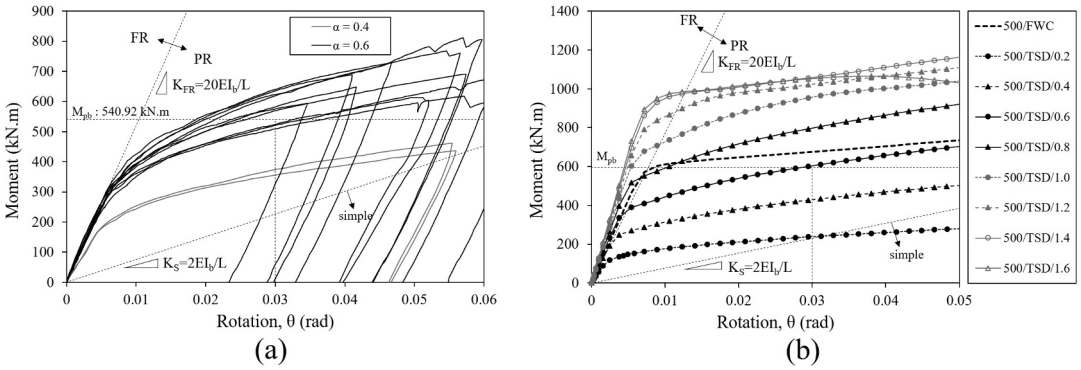

Fig. 30. Connection stiffness evaluation: (a) test results and (b) FEA results (500 series).

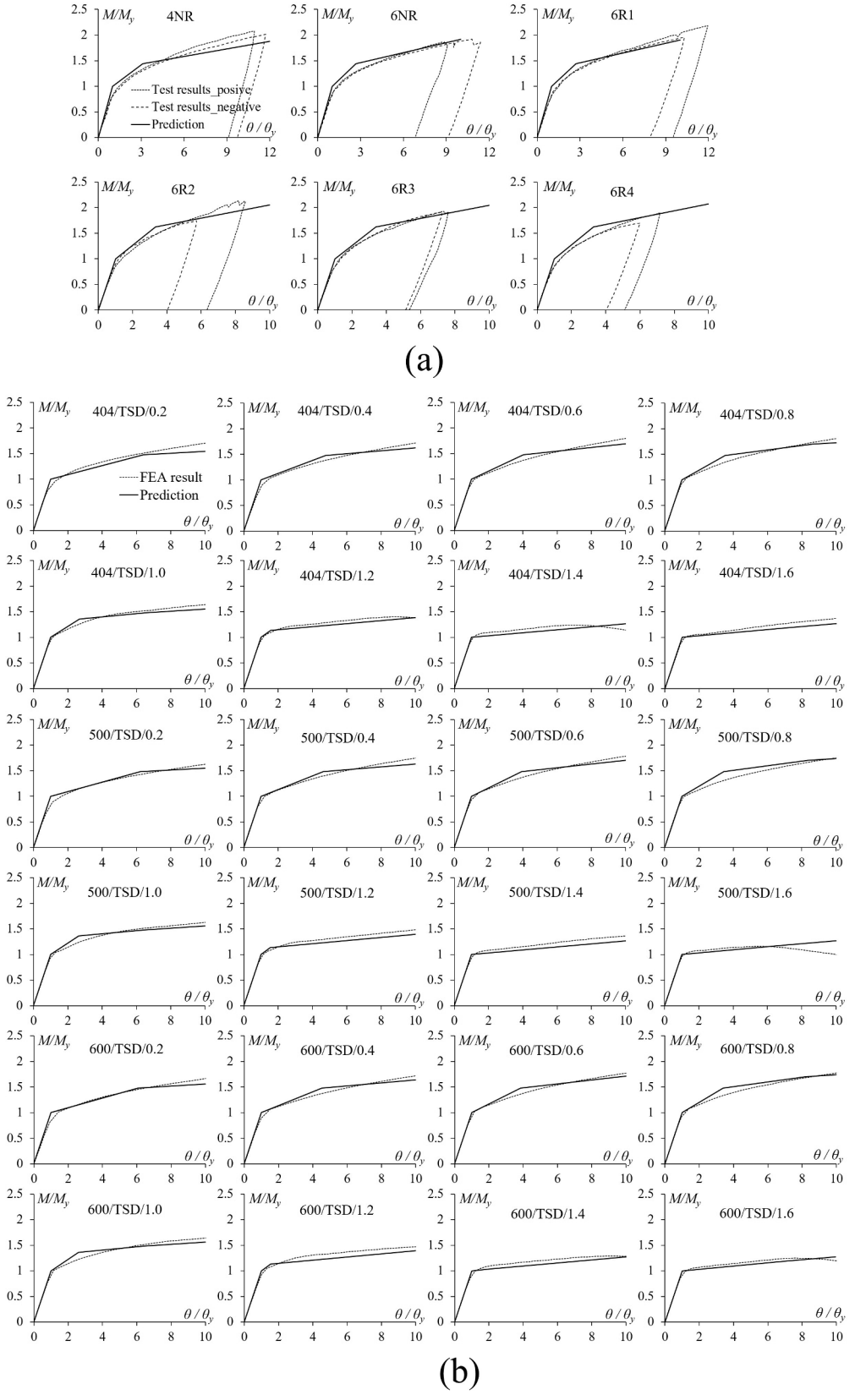

Fig. 33. Comparison between the proposed hysteretic properties and the test/FEA results: (a) test and (b) FEA.

conducted on the beam-to-column connection. Multivariate nonlinear finite element analysis was also conducted to evaluate the structural performance of the proposed system according to the damper/beam yield strength ratio. The conclusions are summarized below.

(1) The TSD beam system effectively followed the characteristics of the existing beam-to-column connection-type damage-controlled system. Owing to the rotational behavior of the connection, deformation was concentrated on the damper, and the overall

behavior exhibited stable hysteresis loops. Moreover, equal resistance was achieved for loadings in both the positive and negative directions.

(2) The 6R4 specimen, which have relatively small aspect ratio (H/B) of the damper showed vulnerable ductility compared to other specimens. The aspect ratio of the damper sufficient to induce flexural yielding is required to secure the ductility of the whole connection. Except for 6R4, with a relatively higher aspect ratio of the damper, the specimens with a damper/beam yield strength ratio of 0.6 exhibited strengths higher than 80% of the full plastic moment of the beam up to a rotation angle of 0.04 rad. These specimens satisfied the requirements for the SMF.

(3) In the test and FEA results, the yield strength of the TSD beam system agreed well with the approximation value. The maximum strength of the TSD beam system, which was appropriately designed to determine the failure mode as the fracture of the damper, was found to be approximately twice the yield strength because the ratio of the ultimate strength to the yield strength of the damper material significantly affected the strength of the system, which differed from the characteristics of typical flexural members.

(4) As the strength of TSD increases in comparison with that of the beam, it is easy to secure the required strength; however, it may be accompanied with plasticity of the beam member. The performance curve for the correlation of strength of the beam system and damage to the beam according to the damper/beam yield strength ratio was derived by analyzing the FEA results. From the curve, an appropriate damper/beam yield strength ratio can be adopted according to actual application requirements.

(5) The stiffness values predicted by the proposed formula were very similar to those of the test and FEA results. In addition, the design stiffness of the TSD beam system is expected that it can achieve the fixation on the level of an FR or PR connection in accordance with AISC.

(6) Moreover, the hysteretic model of the TSD beam system was derived based on the proposed strength and stiffness prediction methods. It was confirmed that the model provided results that were consistent with those of the test and FEA. The proposed hysteretic model could be expressed as a tri-linear model in an approximate manner. The primary variables that determined the characteristic value were identified as the yield ratio of the damper material, the damper/beam yield strength ratio, and the effective length of the beam.

This study proposed modified details for a beam-to-column connection-type damage-controlled system and provides a design methodology for low- and mid-rise steel structures. However, the design variables addressed are not sufficient to meet a wide range of design conditions. Therefore, a follow-up study on the effect of beam effective length and bolt tightening force, etc. is required.

Declaration of Competing Interest

The authors declared that there is no conflict of interest.

Acknowledgements

This research was supported by the Basic Science Research Program through the National Research Foundation of Korea (NRF) funded by the Ministry of Education (2017R1D1A3B03036186).

References

[1] Symans MD, Charney FA, Whittaker AS, Constantinou MC, Kircher CA, John MW, et al. Energy dissipation systems for seismic applications: Current practice and recent developments. J Struct Eng 2008;134(1):3–21.
[2] Benavent-Climent A. A brace-type seismic damper based on yielding the walls of hollow structural sections. Eng Struct 2010;32:1113–22.
[3] Takeuchi T, Tsumagari K, Suzuki K, Saeki E, Yamada S, Wada A. Design and performance of passively controlled building with elasto-plastic damper at beam ends. AIJ J Technol Des 2004;20:125–30. [in Japanese].
[4] Takeuchi T, Shirabe H, Yamada S, Kishiki S, Suzuki K, Saeki E, et al. Cumulative deformation capacity and damage evaluation for elasto-plastic dampers at beam ends. J Struct Constr Eng 2006;600:115–22. [in Japanese].
[5] AISC 358-16, Prequalified Connections for Special and Intermediate Steel Moment Frames for Seismic Applications, ANSI/AISC; 2016.
[6] Oh SH, Kim YJ, Ryu HS. Seismic performance of steel structures with slit dampers. Eng Struct 2009;31:1997–2008.
[7] Saffari H, Hedayat AA, Poorsadeghi-Nejad M. Post-Northridge connections with slit dampers to enhance strength and ductility. J Constr Steel Res 2013;80:138–52.
[8] Oh SH, Park HY. A study on beam-to-column connections with plate type energy absorption system. J. Korean Soc Steel Constr 2013;25(1):93–104. [in Korean].
[9] Oh SH, Park HY. Evaluation of strength and stiffness of the damper installed at beam end for damage-controlled structures. J Archit Inst Korea Struct Constr 2017;33(2):27–36. [in Korean].
[10] Koetaka Y, Chusilp P, Zhang Z, Ando M, Suita K, Inoue K, et al. Mechanical property of beam-to-column moment connection with hysteretic dampers for column weak axis. Eng Struct 2005;27:109–17.
[11] MacRae GA, Clifton GC, Mackinven H, Mago N, Butterworth J, Pampanin S. The sliding hinge joint moment connection. Bull New Zealand Soc Earthquake Eng 2010;43(3):202–12. [in New Zealand].
[12] Latour M, Rizzano G. Design of X-shaped double split tee joints accounting for moment-shear interaction. J Constr Steel Res 2015;104:115–26.
[13] Bayat K, Shekastehband B. Seismic performance of beam to column connections with T-shaped slit dampers. Thin-Walled Struct 2019;141:28–46.
[14] Benavent-Climent A, Oh SH, Akiyama H. Ultimate energy absorption capacity of slit-type steel plates subjected to shear deformations. J Struct Constr Eng 1998;503:139–47. https://doi.org/10.3130/aijs.63.139_1. [in Japanese].
[15] Benavent-Climent A. Influence of hysteretic dampers on the seismic response of reinforced concrete wide beam-column connections. Eng Struct 2006;28(4):580–92.
[16] Chan RWK, Albermani F. Experimental study of steel slit damper for passive energy dissipation. Eng Struct 2008;30(4):1058–66. https://doi.org/10.1016/j.engstruct.2007.07.005.
[17] AISC 341-16, Seismic Provisions for Structural Steel Buildings, ANSI/AISC; 2016.
[18] Kato B, Akiyama H, Yamanouchi H. Predictable properties of structural steels subjected to incremental cyclic loading. In: IABSE Symposium on resistance and ultimate deformability of structures acted on by well defined loads; 1973. p. 119–24.
[19] ANSYS/DYNA, User's manual(Version 16.0). ANSYS, Inc.; 2015.
[20] Mahin SA. Lessons from damage to steel buildings during the Northridge earthquake. Eng Struct 1998;20(4–6):261–70.
[21] Nakashima M, Inoue K, Tada M. Classification of damage to steel buildings observed in the 1995 Hyogoken- Nanbu earthquake. Eng Struct 1998;20(4–6):271–81.
[22] Lee MH, Oh SH, Yoon MH. Energy absorption capacity of X-type braced frame with steel plate slit dampers. J Archit Inst Korea Struct Constr 2009;25(11):53–60. [in Korean].
[23] El-Tawil S, Mikesell T, Vidarsson E, Kunnath S. Strength and ductility of FW welded-bolted connections. Report No. SAC/BD-98/01, SAC Joint Venture, Sacramento, California; 1998.
[24] FEMA-355D, State of the art report on connection performance. (Washington, DC); 2000.
[25] AISC 360-16, Specification for Structural Steel Buildings, ANSI/AISC; 2016.
[26] Hwang SC, Yang IS. Restoring force characteristics model proposal H-section steel beam for dynamic response analysis. J Archit Inst Korea Struct Constr 2007;23(11):35–42. [in Korean].